Tuning carbohydrate density enhances protein binding and inhibition by glycosylated β-sheet peptide nanofibers

Journal:	*Biomaterials Science*
Manuscript ID	BM-ART-05-2018-000533.R1
Article Type:	Paper
Date Submitted by the Author:	03-Jul-2018
Complete List of Authors:	Restuccia, Antonietta; University of Florida, Biomedical Engineering Hudalla, Gregory; University of Florida, Biomedical Engineering

Biomaterials Science

ARTICLE

Tuning carbohydrate density enhances protein binding and inhibition by glycosylated β-sheet peptide nanofibers

Received 00th January 20xx,
Accepted 00th January 20xx

DOI: 10.1039/x0xx00000x

www.rsc.org/

Antonietta Restuccia[a] and Gregory A. Hudalla[a,*]

Carbohydrate-modified biomaterials are attractive for disrupting natural protein-glycan binding events because they present ligands in multivalent arrangements that can address the weak affinity of monovalent protein-carbohydrate interactions. However, protein binding depends on physical aspects of immobilized carbohydrate display, such as density and valency, which are often difficult to predict and can vary for different types of biomaterials. Here, we characterized protein interactions with β-sheet peptide nanofibers with tunable immobilized carbohydrate content, which were prepared by co-assembling QQKFQFQFEQQ (Q11) with a glycosylated variant modified with N-acetylglucosamine (GQ11) at different molar ratios. Rate of protein binding increased as carbohydrate density decreased, with nanofibers having a GQ11:Q11 molar ratio of 1:3 reaching equilibrium faster than formulations with GQ11 mole fraction of 1. A larger protein demonstrated a lower extent of binding than a smaller protein, however, the optimal range of carbohydrate densities was independent of protein size. Nanofibers with the highest apparent protein binding affinity inhibited T cell death induced by wheat germ agglutinin (WGA) more effectively than sub-optimal formulations, because they bound more protein within biologically-relevant time frames (min to h). Collectively, these observations suggest that tuning carbohydrate density via co-assembly of glycosylated and non-glycosylated Q11 variants can maximize multivalent avidity effects while minimizing steric penalties. We anticipate that this approach will enable rapid iterative development of biomaterials with optimal activity for inhibiting protein-glycan interactions implicated in disease progression.

Introduction

Protein-carbohydrate interactions are gaining interest as drug targets due to growing appreciation of their role in various pathological processes, including bacterial and viral infection,[1, 2] cancer,[3, 4] inflammation,[5] and autoimmunity.[6] Carbohydrates and synthetic derivatives are attractive lead compounds for developing selective and specific inhibitors,[7] however, their effectiveness is often limited by the weak binding affinity of monovalent protein-carbohydrate interactions (K_D ~ 10^{-3} – 10^{-6} M). In nature, protein-carbohydrate interactions are stabilized by avidity effects resulting from multiple independent binding events that collectively increase apparent binding affinity.[8] For example, chelate effects observed when multivalent carbohydrates can occupy multiple binding sites on a single protein lower the entropic cost of protein-ligand association. Likewise, statistical rebinding describes the increased probability of proteins to associate with ligands in close proximity rather than dissociate and diffuse away. Characteristic examples of statistical rebinding are soybean agglutinin and Vatairea macrocarpa lectin association with porcine submaxillary mucins, in which apparent binding affinity increases with glycoprotein chain length.[9] Often referred to as the 'cluster glycoside effect',[10] carbohydrate multivalency is becoming increasingly important for designing inhibitors of protein-carbohydrate interactions.

Various types of biomaterials are used as scaffolds to mimic natural multivalent carbohydrate presentation, including polymers, nanoparticles, proteins, polypeptides, and dendrimers.[11-13] Prior work has demonstrated that protein recognition by immobilized carbohydrates depends on scaffold features, such as architecture, linker length, and rigidity, as well as carbohydrate density (i.e., lateral distance between carbohydrates) and carbohydrate valency (i.e., total number of carbohydrate molecules on the scaffold).[14, 15] Many examples of biomaterials modified with carbohydrates (i.e., "glycomaterials") that can enhance or inhibit the biological activity of protein targets have been reported to date.[16-18] Critical to these advances is establishing design guidelines that correlate physical and chemical properties of different glycomaterial scaffolds with their protein binding properties.[19-27] Thus, ideal glycomaterials provide simple, user-defined control of carbohydrate density and valency on a single scaffold architecture to enable systematic optimization of protein binding affinity, specificity, and kinetics according to the intended biomedical or biotechnological application.

Carbohydrate-modified molecules that self-assemble into supramolecular structures are receiving increasing attention as glycomaterials.[28-37] For example, we recently reported β-sheet peptide nanofibers modified with a disaccharide that can specifically recognize galectins, a family of soluble carbohydrate-binding proteins.[38] Self-assembled peptide nanofibers are advantageous as scaffolds for immobilized ligands because their molecular composition is easily interchangeable, can be finely tuned, and is

[a] J. Crayton Pruitt Family Department of Biomedical Engineering, University of Florida, Gainesville, FL, USA 32611.
*PO Box 116131, Biomedical Sciences JG56, 1275 Center Drive, Gainesville, FL, USA, 32611, (352)273-9326, ghudalla@bme.ufl.edu
Electronic Supplementary Information (ESI) available: [details of any supplementary information available should be included here]. See DOI: 10.1039/x0xx00000x

robustly reproducible.[39] For example, variants of the β-sheet fibrillizing peptide QQKFQFQFEQQ (Q11) modified with different ligands can be co-assembled at optimal ratios to elicit desired biological responses, such as cell adhesion and proliferation,[40] or adaptive immunity.[41] However, relationships between the composition of carbohydrates immobilized onto self-assembled peptide nanofibers and their protein binding properties are poorly defined. Here, we systematically characterized relationships between the density and valency of carbohydrates on Q11 nanofibers and their recognition of carbohydrate-binding proteins. Specifically, we co-assembled Q11 and a variant modified with the monosaccharide n-acetylglucosamine (i.e., "GQ11") at different molar ratios to create nanofibers with a broad range of carbohydrate densities (Fig. 1a-b). We expected that tuning carbohydrate density would increase protein binding affinity by maximizing statistical rebinding while minimizing steric penalties (Fig. 1c). As a model system, we characterized GQ11 nanofiber binding to two plant lectins that recognize N-acetylglucosamine (GlcNAc), wheat germ agglutinin (WGA) and Griffonia Simplicifolia lectin II (GS II). We established relationships between carbohydrate density on the nanofiber and lectin binding rate, as well as relationships between valency, density, and extent of protein binding. We also evaluated the efficacy of GQ11 nanofibers to inhibit WGA-induced T cell death in vitro as a function of carbohydrate density. The results from this study illustrate the potential of peptide co-assembly to easily and rapidly survey glycomaterials with user-defined carbohydrate content to identify optimal multivalent lectin inhibitors.

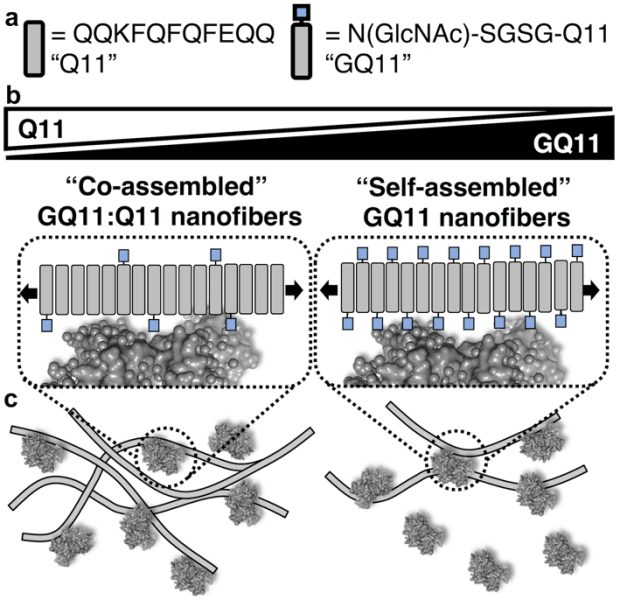

Figure 1. Schematic representation of glycosylated β-sheet peptide nanofibers that can capture carbohydrate-binding proteins. (a) Q11 and the glycosylated Q11 variant, N(GlcNAc)-SGSG-QQKFQFQFEQQ (GQ11). (b) Co-assembled nanofibers of Q11 and GQ11 have lower carbohydrate density than self-assembled GQ11 nanofibers. (c) Bound proteins, such as wheat germ agglutinin (WGA), are expected to sterically shield more carbohydrates on GQ11 nanofibers than GQ11:Q11 nanofibers, leading to lower effective carbohydrate concentration that decreases apparent binding affinity.

Results and Discussion

WGA binding by glycosylated peptide nanofibers is optimal at moderate carbohydrate density and valency

We characterized lectin binding to nanofibers with different carbohydrate densities by co-assembling GQ11 and non-glycosylated Q11 at different molar ratios, reported as (GQ11:Q11) (Fig. S3). First, binding kinetics were determined using a turbidity assay in which crosslinking of lectin and nanofibers into insoluble networks leads to measurable attenuation of incident light.[19] Nanofibers with low carbohydrate density (250:750) formed macroscopic aggregates within minutes when incubated with WGA (Fig. 2a, black circles). In contrast, nanofibers with equivalent carbohydrate valency at high density (250:0) formed macroscopic aggregates much more slowly in the presence of WGA, taking more than 18 hours to reach maximum visible light attenuation (Fig. 2a, white squares). When total peptide concentration was held constant, nanofibers with high carbohydrate density and valency (1000:0) formed aggregates more slowly than nanofibers with low carbohydrate density and valency (250:750) (Figure S4). Collectively, these observations suggested that kinetics of lectin binding to glycosylated peptide nanofibers were more dependent on immobilized carbohydrate density than valency.

To relate aggregate formation kinetics with lectin binding affinity, we characterized extent of WGA binding to glycosylated peptide nanofibers at different time points. We used an established sedimentation assay,[38] in which nanofibers plus bound lectin are first separated from unbound lectin via centrifugation, and then unbound lectin in the supernatant is measured fluorimetrically. 250:750 nanofibers bound more than 95% of WGA in solution after 1 h of incubation, whereas 250:0 nanofibers bound less than 60% of WGA in solution (Figure 2b). Concentration of WGA bound to 250:750 nanofibers was unchanged after 24 h, whereas WGA concentration bound to 250:0 nanofibers increased to an extent approximately equal to that bound to 250:750 nanofibers. Taken together, these data demonstrated that glycosylated peptide nanofibers having relatively low carbohydrate density reached binding equilibrium with WGA faster than nanofibers with high carbohydrate density.

To further understand relationships between carbohydrate density and valency, we compared WGA binding to a library of GQ11:Q11 and GQ11 nanofibers. First, we compared WGA binding to GQ11:Q11 nanofibers for which valency and density are coupled to

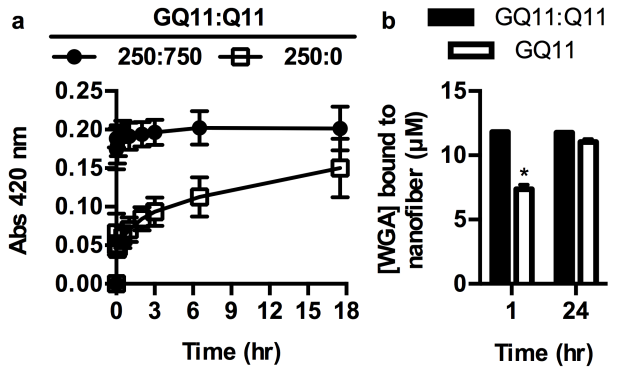

Figure 2. Carbohydrate density on Q11 nanofibers determines WGA binding kinetics. (**a**) Turbidity assay demonstrating that co-assembled GQ11:Q11 nanofibers having lower carbohydrate density aggregate faster in the presence of WGA than GQ11 nanofibers having equivalent carbohydrate valency at high density. (**b**) Co-precipitation assay demonstrating that GQ11:Q11 nanofibers having lower carbohydrate density reach binding equilibrium with WGA faster than GQ11 nanofibers having equivalent carbohydrate valency at high density. * $p < 0.005$, student's t-test.

GQ11 nanofibers with a range of GlcNAc valencies at high density. Both nanofiber formulations bound a comparable amount of WGA at high GlcNAc valency (i.e., [GQ11] ≥ 500 μM), however, GQ11:Q11 nanofibers approached maximum binding at lower valency than GQ11 nanofibers (Fig. 3a). Scatchard analysis of these saturation binding data yielded negative linear trends (Fig. 3b), suggesting non-cooperative association of WGA with these GQ11 and GQ11:Q11 nanofiber formulations. Non-linear regression of saturating binding data estimated that GQ11:Q11 nanofiber dissociation constant (K_D) for WGA was ~3-fold lower than that of GQ11 (Fig. 3c), consistent with the steeper slope for the Scatchard plot of GQ11:Q11 nanofibers. Together, these observations demonstrated that decreasing immobilized glycan density on Q11 nanofibers increased WGA binding affinity, consistent with observations that decreasing glycan density can enhance lectin binding rate (Fig. 2).

Next, we compared WGA binding to GQ11:Q11 nanofibers with equivalent GlcNAc valency at different densities. Extent of WGA binding increased to a maximum as GlcNAc density was decreased (i.e., [Q11] was increased), although extent of WGA binding was significantly diminished at very low GlcNAc densities (i.e., high [Q11]) (Fig. 3d). Similarly, when the GlcNAc to WGA ratio was held constant to normalize the driving force for binding, GQ11:Q11 nanofibers with a moderate GlcNAc density and valency demonstrated the highest extent of WGA binding (Fig. 3e). Taken together, these observations suggested that nanofibers with moderate glycan density and valency would demonstrate optimal WGA binding affinity. To test this, we characterized WGA binding to GQ11:Q11 nanofibers with low density and valency (100:900), moderate density and valency (250:750), or high density and valency (1000:0). Low density, low valency nanofibers approached saturation at ~15 μM bound WGA (Fig. 4a, black triangles). Strikingly, high density, high valency nanofibers bound nearly the same amount of WGA over 1 h as low density, low valency nanofibers (Fig. 4a, white squares), despite a 10-fold difference in carbohydrate content, further supporting observations that increasing carbohydrate density decreases lectin binding rate (Fig. 2). In contrast, nanofibers with moderate carbohydrate density and valency were not saturated over the range of 2.5-25 μM WGA (Fig. 4a, black circles). Scatchard analysis suggested that WGA binding to 100:900 and 1000:0 nanofibers was not cooperative (Fig. 4b), where the latter was consistent with WGA binding to high density nanofibers at a range of valencies (Fig. 3b). Non-linear regression estimated an ~2-fold difference in K_D for WGA binding to 100:900 and 1000:0 nanofibers (Fig. 4c), demonstrating that high glycan density did not significantly enhance lectin binding affinity. In contrast, Scatchard analysis suggested positive cooperativity for WGA binding to 250:750 nanofibers (Fig. 4b), which precluded accurate estimation of K_D (Fig. 4c). Notably, this contrasted with the observed non-cooperative binding of WGA to GQ11:Q11 nanofibers with a range of increasing densities and valencies (Fig. 3b). Collectively, these data demonstrated that binding affinity was optimal for nanofibers with moderate carbohydrate density and valency, likely due multivalent avidity effects that maximized statistical rebinding while avoiding steric penalties.

We postulate that the observed differences in rate and extent of WGA binding to glycosylated peptide nanofibers may result from steric masking of neighboring carbohydrates by a bound lectin.[42] In particular, WGA is a dimer with four accessible binding sites and a hydrodynamic diameter of ~56 Å.[43, 44] On the other hand, carbohydrates appended onto β-strands of an anti-parallel β-sheet are ~9.2 Å apart (distance between β-strands is ~4.6 Å),[45] which is approximately one-sixth of the hydrodynamic diameter of the lectin. Co-assembly of GQ11 with diluent Q11 increases the average linear

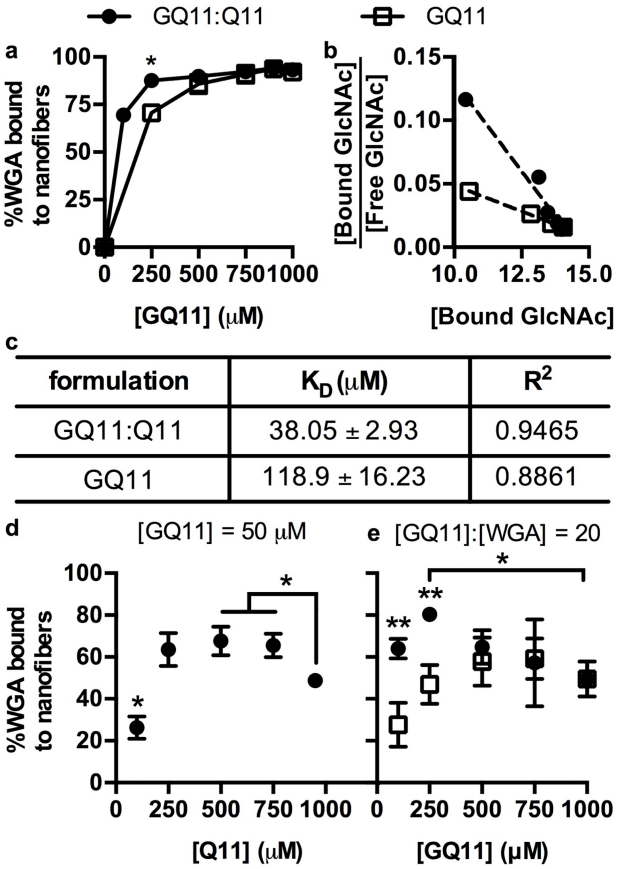

Figure 3. Carbohydrate density on Q11 nanofibers determines extent of WGA binding. (**a**) % WGA bound to GQ11 nanofibers with increasing GlcNAc valency at high density (open squares) or GQ11:Q11 nanofibers with increasing GlcNAc density and valency (GlcNAc density ∝ [GQ11]) (black circles) when $[WGA]_{total}$ = 15 μM. (**b**) Scatchard plots and (**c**) dissociation constants (K_D) determined from data in (a). (**d**) % WGA bound to GQ11:Q11 nanofibers with equivalent valencies at different densities when $[WGA]_{total}$ = 2.5 μM (GlcNAc density ∝ 1/[Q11]). (**e**) Comparison of % WGA bound to GQ11 nanofibers with different GlcNAc valency (open squares) or GQ11:Q11 nanofibers with different GlcNAc density and valency (black circles) when the GQ11 to WGA ratio was held constant at 20 ([WGA] = 5, 12.5, 25, 37.5, and 50 μM, respectively). In all experiments, total peptide (GQ11 + Q11) = 1 mM for GQ11:Q11 group. In (a) * represents $p < 0.05$, and in (d) and (e) ** represents $p < 0.01$, student's t-test comparing GQ11:Q11 to GQ11 at [GQ11]. In (d) and (e), * represents $p < 0.05$ compared to all other conditions unless indicated otherwise, ANOVA with Tukey's post-hoc.

distances between carbohydrates on the nanofiber, thereby decreasing the number of glycans masked by a bound lectin (Fig. 1c). Thus, "effective" carbohydrate concentration would decrease more rapidly as a function of lectin binding to GQ11 than GQ11:Q11 nanofibers. Since association rate is dependent on the microaffinity constant, which is dependent on the effective concentration of both protein and ligand in solution, a more rapid decrease in effective carbohydrate concentration on GQ11 nanofibers would explain their slower binding rate compared to GQ11:Q11 nanofibers. Similar effects have been reported for soybean agglutinin lectin association with submaxillary mucins, where microaffinity constant decreases as extent of lectin binding increases.[46, 47]

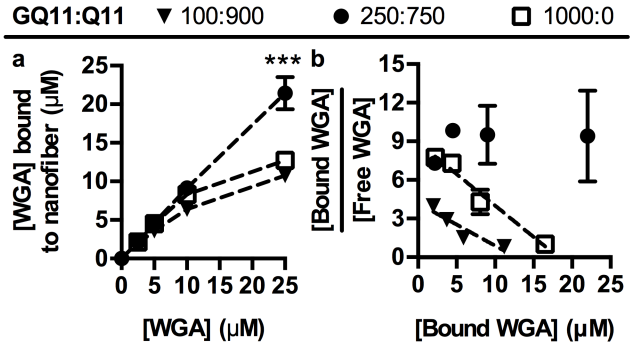

c formulation	K_D (μM)	R^2
100:900	38.05 ± 2.93	0.9806
250:750	N.D.	N.D.
1000:0	19.03 ± 2.43	0.9875

Figure 4. Extent of WGA binding is maximized on Q11 nanofibers with moderate glycan density and valency. (a) WGA concentration bound to low density, low valency (100:900), moderate density, moderate valency (250:750), or high density, high valency (1000:0) GQ11:Q11 nanofibers. (b) Scatchard plots and (c) K_D determined from data in (a). *** denotes $p < 0.001$, ANOVA with Tukey's post-hoc.

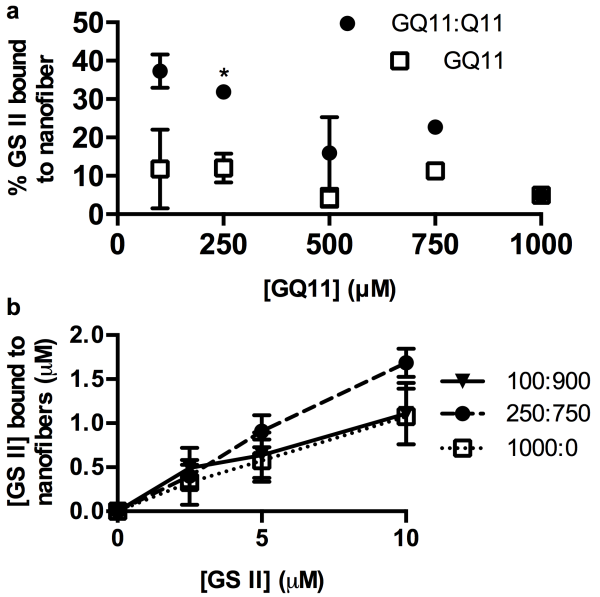

Figure 5. Extent of GS II binding is maximized on Q11 nanofibers with moderate carbohydrate density and valency. (a) Co-precipitation assay demonstrating extent of GS II binding to GQ11:Q11 and GQ11 nanofibers as a function of GQ11 concentration. (b) Co-precipitation assay demonstrating amount of GS II bound to GQ11:Q11 nanofibers with different densities and valencies as a function of GS II concentration. * denotes $p < 0.05$, student's t-test.

GS II binding by glycosylated peptide nanofibers is optimal at moderate carbohydrate density and valency

We characterized GQ11 nanofiber recognition of another GlcNAc-binding protein, *Griffonia Simplicifolia* lectin II (GS II), to determine if the observed relationships between carbohydrate content on Q11 nanofibers and their lectin binding properties were specific to WGA. GQ11:Q11 nanofibers with lower density and valency (i.e., [GQ11] < 500 μM) bound more GS II than nanofibers with high density, regardless of valency (Fig. 5a). Likewise, 250:750 nanofibers demonstrated a tendency to bind more GS II at increasing lectin concentrations than 100:900 and 1000:0 nanofibers (Figure 5b), which bound comparable amounts of GS II despite having a 10-fold difference in GlcNAc valency. Previous studies using brush-like glycopolymers also demonstrated that GS II binding kinetics and equilibrium dissociation constant were dictated by scaffold topology and overall glycan accessibility.[48] Here, we assume that differences in the extent of WGA and GS II binding to glycosylated peptide nanofibers can be attributed to differences in size, as well as orientations and binding preferences of their carbohydrate recognition domains. For example, although both lectins are known to recognize GlcNAc, WGA preferentially binds internal carbohydrate residues within polysaccharides, while GS II binds terminal residues.[49, 50] In our studies, extent of GS II binding to GQ11 nanofibers was significantly lower relative to WGA, regardless of carbohydrate density. This was not surprising, given that the molecular weight of WGA is nearly three times smaller than GS II, which consists of four 30 kDa subunits.[51] Thus, binding of a larger GS II molecule to glycosylated peptide nanofibers would be expected to sterically shield more carbohydrates than a bound WGA molecule. Nonetheless, these observations suggested two general design guidelines for glycosylated β-sheet peptide nanofibers: (1) co-assembly of GQ11 with diluent Q11 enhances protein binding, and (2) optimal lectin binding affinity correlates with a relatively narrow range of glycan densities.

The length of the linker separating GlcNAc from Q11 nanofibers does not influence WGA binding

Previous reports demonstrate that linker length and flexibility can affect lectin binding to multivalent carbohydrates,[52-54] and here we considered that the Q11 nanofiber scaffold may establish steric penalties that hinder WGA binding to immobilized GlcNAc. To probe the influence of the linker separating GlcNAc and Q11 on lectin binding, we characterized WGA interactions with GQ11 variants having a short (~2 nm) linker, referred to as "G-2-Q11", and a long (~8 nm) linker, referred to as "G-8-Q11", where the parent GQ11 molecule has an intermediate (~4 nm) linker. G-2-Q11 and G-8-Q11 formed elongated nanofibers with morphological features and β-sheet content that were similar to GQ11 (Figure 6a-c and S5).[27] Co-assembled nanofibers consisting of 250 μM GQ11 and 750 μM Q11 (i.e. 250:750) bound comparable amounts of WGA after 1 h, regardless of linker length (Fig. 6d), suggesting that the Q11 nanofiber did not impose significant steric penalties on WGA:GlcNAc binding. This was not necessarily surprising since WGA carbohydrate recognition domains are shallow clefts located near the protein surface. Nonetheless, in other contexts, such as GS II binding to GQ11:Q11 nanofibers (Fig. 5) or galectin binding to LacNAcQ11:Q11 nanofibers reported previously,[38] linker length or rigidity may still be an important determinant of binding affinity or binding kinetics.

Although previous reports demonstrate an influence of linker length and rigidity on WGA binding to multivalent carbohydrate ligands, the most drastic effects are associated with scaffold architectures that promote chelate effects, such as calix[n]renes and cyclopeptides.[55, 56] For example, optimal linker lengths can increase apparent WGA-GlcNAc binding affinity ~25,000-fold compared to monovalent GlcNAc alone.[54] In contrast, WGA binding to GlcNAc moieties immobilized onto a surface, which we consider analogous

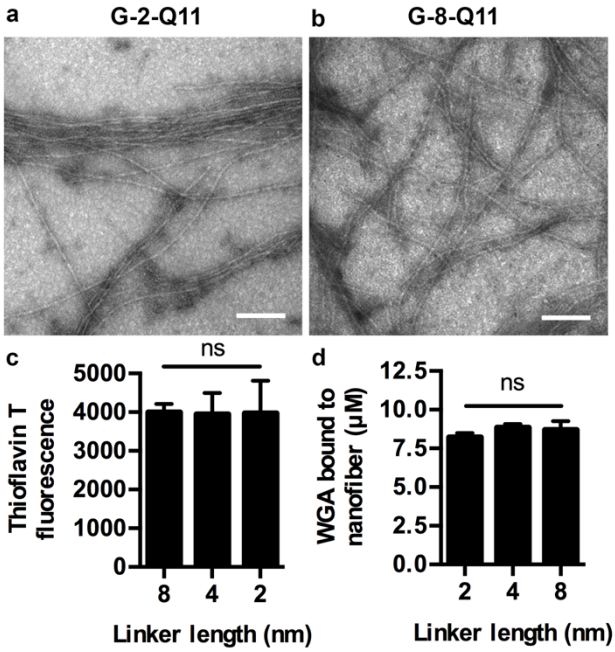

Figure 6: Linker length does not influence WGA binding to co-assembled GQ11:Q11 nanofibers with moderate carbohydrate density and valency. Transmission electron micrographs demonstrating that (a) G-2-Q11 and (b) G-8-Q11 self-assembled into elongated nanofibers with morphologies similar to the parent GQ11 molecule (scale bar = 100 nm). (c) G-2-Q11, parent GQ11 (i.e., G-4-Q11), and G-8-Q11 nanofibers were rich in β-sheets based on ThT fluorescence. (d) Co-precipitation assay demonstrating that GQ11:Q11 nanofibers (250:750) bound comparable amounts of WGA at 1 h regardless of linker length. "ns" represents no significant difference using ANOVA with Tukey's post-hoc.

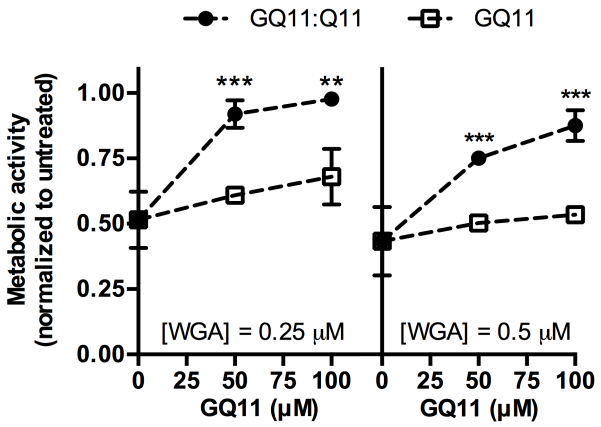

Figure 7. Nanofibers with optimal carbohydrate density inhibited WGA-induced Jurkat T cell death more effectively than nanofibers with high carbohydrate density. Jurkat T cell metabolic activity, a measure of viability, in the presence of 250:750 GQ11:Q11 nanofibers or 250:0 GQ11 nanofibers in media supplemented with (a) 0.25 μM or (b) 0.5 μM WGA. ** represents $p < 0.01$ and *** represents $p < 0.001$, student's t-test.

to GQ11 nanofibers, are less clear.[57] For example, immobilizing GlcNAc onto Q11 nanofibers only increased binding affinity by ~85-90 fold when compared to monovalent GlcNAc (K_D ~20-30 μM (Fig. 4c) vs 2.5 mM,[58] respectively). We infer that chelate effects are unlikely to be a major contributor to protein-nanofiber binding. Rather, we postulate that the increased binding affinities reported herein are due to a combination of statistical rebinding effects endowed by carbohydrate multivalency (i.e. 'bind and slide'), as well as decreased entropic penalties due to immobilizing GlcNAc onto a Q11 nanofiber. Elucidating the thermodynamic parameters governing lectin binding to glycosylated peptide nanofibers, which are beyond the scope of this report, will likely aid in clarifying these contributions.

Nanofibers that rapidly bind lectin are more effective inhibitors

We characterized relationships between GQ11 nanofiber apparent WGA binding affinity and potency for inhibiting WGA biological activity using an *in vitro* Jurkat T cell death assay. Co-assembled GQ11:Q11 nanofibers (250:750) inhibited WGA-induced Jurkat T cell death more effectively than GQ11 nanofibers at two different WGA concentrations (Fig. 7a-b). In all cases, GlcNAc concentration was at least 200-fold greater than WGA concentration, an excess expected to be sufficient to saturate WGA binding sites. Indeed, under these conditions, both GQ11:Q11 and GQ11 nanofibers bound equivalent amounts of WGA at equilibrium, but their lectin binding rates differed (Fig. 2). Taken together, these observations demonstrated that glycosylated peptide nanofibers that bind WGA more rapidly are more effective inhibitors. This was not necessarily surprising since WGA activates pro-apoptotic signaling mechanisms (e.g. inner mitochondrial membrane disruption, cytochrome c release) within 30 minutes of incubation with Jurkat T cells.[59] Thus, these observations underscore the importance of lectin binding rate, in addition to dissociation constant, as a key predictor of multivalent glycoconjugate inhibitory efficacy.

Conclusions

The results presented here demonstrate that protein recognition by glycosylated β-sheet peptide nanofibers depends on carbohydrate density. Glycosylated peptide nanofibers bound comparable amounts of protein at equilibrium, regardless of carbohydrate density, however nanofibers with low to moderate carbohydrate densities reached equilibrium faster than nanofibers with high carbohydrate densities, regardless of valency. Increased rate of lectin binding correlated with improved efficacy for inhibiting WGA-induced T cell apoptosis in vitro. Similar correlations between protein binding and carbohydrate density were observed with two different GlcNAc-binding lectins, suggesting that these relationships were a common feature of glycosylated peptide nanofibers. We attribute the observed density-dependent differences in protein binding to steric masking of carbohydrates. Due to the larger size of proteins relative to carbohydrates, binding of one protein molecule to one carbohydrate molecule within a multivalent cluster can mask multiple neighboring carbohydrates. Thus, the concentration of carbohydrate ligands that are available to bind proteins (i.e. the "effective concentration") will decrease at a faster rate as protein size increases. Consistent with this, the results presented here demonstrated that glycosylated peptide nanofibers bound less GS II, a relatively large lectin, than WGA, which is considerably smaller. Therefore, increasing the distance between neighboring carbohydrates would be expected to enhance protein binding by reducing the number of ligands masked by each bound protein molecule. Consistent with this, we observed higher extent of lectin binding to nanofibers with GQ11:Q11 ratios less than 1 when compared to nanofibers assembled from GQ11 alone or GQ11:Q11

ratios greater than 1. However, nanofibers with carbohydrate densities that were too low demonstrated weakened binding, likely due to diminished avidity effects. Inverse relationships between glycan density and lectin binding have also been reported for glycodendrimersomes,[27] suggesting that optimal affinity at moderate glycan density may be a shared trait among self-assembled glycomaterials. Interestingly, this would distinguish self-assembled glycomaterials from glycopolymers and glyconanoparticles, for which binding affinity and ligand density are often directly related.[19, 21, 24, 60, 61] Future efforts to benchmark lectin binding to different self-assembled glycomaterials are expected to clarify these relationships, ultimately leading to design guidelines for supramolecular biomaterials that bind specific lectin targets with high affinity and rapid kinetics. In total, these observations reinforce the notion that protein recognition by carbohydrates immobilized onto biomaterials depends on physical features that are difficult to predict a priori, highlighting the need for platforms that enable systematic and reproducible tuning of carbohydrate density and valency to define structure-function relationships. Self-assembled glycomaterials, such as the β-sheet peptide nanofibers reported herein, are ideal in this regard because their composition can be finely tuned via modular co-assembly of different molecular building blocks.

Materials and Methods

Peptide synthesis and purification

Amino acids and amide resin were purchased from Novabiochem. 2-(7-Aza-1H-benzotriazole-1-yl)-1,1,3,3-tetramethyluronium hexafluorophosphate (HATU), 1-Hydroxy-7-azabenzotriazole (HOAt), N,N- Diisopropylethylamine (DIEA), dimethylformamide (DMF), trifluoroacetic acid (TFA), diethyl ether, and methanol were purchased from Fisher Scientific. Piperidine, 1,8-Diazabicyclo[5.4.0]undec-7-ene (DBU), triisopropylsilane (TIS), and sodium methoxide were purchased from Sigma-Aldrich. Peptides GQ11 (N(GlcNAc)SGSGQQKFQFQFEQQ), G-2-Q11 (N(GlcNAc)SGQQKFQFQFEQQ), G-8-Q11(N(GlcNAc)SGSGSGSGQQKFQFQFEQQ), and Q11 (QQKFQFQFEQQ), were synthesized following standard Fmoc solid phase peptide synthesis protocols with DIEA/HOAt/HATU activation, according to previously reported methods.[38] Peptides were cleaved with TFA/TIS/water (95:2.5:2.5) cocktail. Peptides were precipitated with diethyl ether, dried, resuspended in distilled water, and freeze dried. GQ11, G-2-Q11, and G-8-Q11 were further treated with sodium methoxide and precipitated in methanol for deacetylation. All peptides were purified using reversed-phase high-performance liquid chromatography (RP-HPLC) on an Ultimate 3000 equipped with a C18 column. Peptide molecular weight was confirmed using MALDI-TOF on a Bruker Microflex LRF system with α-cyano-4-hydroxycinnamic acid as the matrix (Fig. S1). Peptide purity was >95% for all studies (Fig. S2).

Nanofiber preparation

Peptide powders were dissolved in ultrapure water (5 mM), diluted to working concentration in 1x phosphate buffered saline (PBS) (137 mM NaCl, 2.7 mM KCl, 10 mM Na_2HPO_4, 1.8 mM KH_2PO_4), and incubated for at least 12 hours. To prepare nanofibers with different carbohydrate densities, GQ11 and Q11 peptide powders were mixed at different molar ratios and dissolved in water to induce co-assembly, similar to established methods.[62] Sample labels indicate the molar concentration (in μM) of GQ11 and Q11. For example, a nanofiber with 250 μM GQ11 and 750 μM Q11 is labeled 250:750, and the total peptide concentration is the sum of the two components (1000 μM).

We used an RP-HPLC assay to determine the GlcNAc content of GQ11:Q11 nanofibers, similar to previous methods.[38] GQ11 and Q11 were mixed as dry powders at different molar ratios, dissolved in water as described above, diluted 10-fold in 1x PBS to a final concentration of 3.2 mM, and incubated for 30 min. Nanofibers were then sedimented by centrifugation at 12000 xg for 5 min. Greater than 90% of peptide in solution was sedimented by centrifugation, independent of carbohydrate content (data not shown), consistent with previous reports.[63] Following centrifugation, supernatant above the nanofiber pellet was carefully removed via pipet, nanofibers were resuspended in TFA, and nanofibers were disassembled via vigorous pipetting. GQ11 and Q11 content in each TFA solution was then independently analyzed via RP-HPLC using an Ultimate 3000 HPLC equipped with a C18 column. An RP-HPLC chromatogram was collected from each sample containing a mixture of GQ11 and Q11 in TFA. The area under the GQ11 peak (~18.5 min; confirmed via MALDI-TOF-MS) and Q11 peak (~19.5 min; confirmed via MALDI-TOF-MS) was calculated. RP-HPLC chromatograms of serial dilutions of TFA solutions with known concentrations of GQ11 or Q11 were then collected and the area under the GQ11 or Q11 peak was used to create standard curves of absorbance vs. GQ11 concentration or Q11 concentration, respectively. Standard curves were used to convert the area under the Q11 or GQ11 peak in each sample RP-HPLC chromatogram to peptide concentration in the sample, and mole fraction of GQ11 in each sample was then calculated from these concentrations. Chromatograms from each GQ11:Q11 mole fraction were collected for three replicates, and all standards were run in duplicate.

Turbidimetric assays

Turbidity measurements were performed to investigate kinetics of lectin binding to nanofibers. Assays were adapted from previously reported methods.[19] 100 μL of (250:750) and (250:0) nanofibers in PBS were incubated at room temperature with 12.5 μM WGA. Absorbance was recorded over time at 420 nm using a SpectraMax M3 spectrophotometer (Molecular Devices). Samples were run in triplicates. The curve represents the average and standard deviation of all three measurements.

Co-precipitation assays to determine lectin binding to nanofibers

Nanofibers were incubated at room temperature with wheat germ agglutinin (WGA, Sigma L9640) or Griffonia Simplicifolia Lectin II (GS II, Vector Laboratories L-1210) for 1 hour unless stated otherwise. Nanofibers were sedimented by centrifugation at 11,300 x g for 5 min. Unbound protein in the supernatant was quantified by measuring tryptophan fluorescence using a SpectraMax M3 spectrophotometer (excitation = 280 nm and emission = 345 nm). Fluorescence signals were converted to lectin concentration using calibration curves respective to each lectin. Scatchard plots were prepared by calculating the ratio of bound WGA concentration to free WGA concentration and then plotting these values against the bound WGA concentration, or calculating the ratio of bound GlcNAc concentration to free GlcNAc concentration and then plotting these values against bound GlcNAc concentration. Bound/free WGA or GlcNAc concentration ratios were calculated for each experimental replicate and then averaged. Data are reported as this average ± standard deviation. Linear regression was performed using GraphPad Prism software. Dissociation constants were extracted via non-linear regression of saturating binding data using the one-site binding model (hyperbola) in GraphPad Prism software.

Transmission electron microscopy

G-2-Q11 and G-8-Q11 nanofibers we adsorbed onto Formvar/carbon grids (FCF400-CU-UB, Electron Microscopy Sciences) from a droplet containing 250 μM peptide in PBS. Grids were dried by tilting onto a Kimwipe™ (Kimberly-Clark). Samples were then negatively stained with a 2% aqueous solution of uranyl acetate. Samples were imaged on a Hitachi-7000 maintained by the UF Interdisciplinary Center for Biotechnology Research.

Thioflavin T staining

β-sheet content of GQ11, G-2-Q11 and G-8-Q11 samples was quantified using Thioflavin T (ThT) (Acros Organics), similar to previously reported methods.[64] Nanofibers were prepared as described above, diluted to 1 mM in PBS, and mixed with aqueous Thioflavin T solution (0.8 mM) at a 10:1 ratio. Fluorescence was measured using a SpectraMax M3 spectrophotometer (excitation = 385 nm, emission = 450 nm).

Fourier transform infrared spectroscopy (FTIR)

Peptides secondary structure was characterized using attenuated total reflectance (ATR) FTIR. A 3 μL nanofiber solution in water (5 mM) was deposited onto a diamond-coated ZnSe crystal and dried at room temperature. Spectra were collected with a PerkinElmer Spectrum 100 spectrometer equipped with a KBr beam splitter. The data presented corresponds to the average of 4 scans at a resolution of 4 cm^{-1}.

Nanofiber inhibitory activity in vitro

Jurkat T cells (E6-1) (ATCC) were kindly provided by Dr. Benjamin Keselowsky. Jurkat T cells were grown in RPMI media supplemented with 10% Fetal Bovine Serum (FBS) (Hyclone), 1% penicillin-streptomycin (Gibco), 200 mM L-glutamine (HyClone), and 1% HEPES buffer (Hyclone), at 37 °C and 5% CO_2. Jurkat T cells (30,000 cells/mL) were incubated with 0.25 or 0.5 μM WGA and increasing concentrations of 250 μM GQ11 or 250:750 GQ11:Q11 nanofibers overnight. Previous studies demonstrated that Q11 and GQ11 nanofibers do not induce Jurkat T cell apoptosis,[38] and therefore control samples of nanofibers alone were not included here. Cell metabolic activity, used here as a measure of viability, was determined using the Cell-Titer Blue assay (Promega), according to the manufacturer's instructions.

Statistical analysis

All experimental and control groups consisted of 3 independent replicates for WGA turbidimetric assays, WGA and GS II co-precipitation assays, and Jurkat T cell apoptosis assays. All studies were performed in duplicate. Statistical differences between groups were analyzed using student t-test (2 groups) or one-way ANOVA with Tukey's post hoc (multiple groups) using GraphPad Prism software.

Conflicts of interest

There are no conflicts to declare.

Acknowledgements

This research was supported by NSF Career (DMR-1455201) to G.A.H.

Notes and references

1. K. A. Karlsson, *Biochem Soc Trans*, 1999, **27**, 471-474.
2. A. E. Smith and A. Helenius, *Science*, 2004, **304**, 237-242.
3. D. H. Dube and C. R. Bertozzi, *Nat Rev Drug Discov*, 2005, **4**, 477-488.
4. P. Nangia-Makker, J. Conklin, V. Hogan and A. Raz, *Trends Mol Med*, 2002, **8**, 187-192.
5. Y. van Kooyk and G. A. Rabinovich, *Nat Immunol*, 2008, **9**, 593-601.
6. G. A. Rabinovich and D. O. Croci, *Immunity*, 2012, **36**, 322-335.
7. B. Ernst and J. L. Magnani, *Nat Rev Drug Discov*, 2009, **8**, 661-677.
8. C. Fasting, C. A. Schalley, M. Weber, O. Seitz, S. Hecht, B. Koksch, J. Dernedde, C. Graf, E. W. Knapp and R. Haag, *Angew Chem Int Ed Engl*, 2012, **51**, 10472-10498.
9. T. K. Dam, T. A. Gerken, B. S. Cavada, K. S. Nascimento, T. R. Moura and C. F. Brewer, *J Biol Chem*, 2007, **282**, 28256-28263.
10. J. J. Lundquist and E. J. Toone, *Chem Rev*, 2002, **102**, 555-578.
11. M. Delbianco, P. Bharate, S. Varela-Aramburu and P. H. Seeberger, *Chem Rev*, 2016, **116**, 1693-1752.
12. R. J. Pieters, *Org Biomol Chem*, 2009, **7**, 2013-2025.
13. M. Delbianco, A. Kononov, A. Poveda, Y. Yu, T. Diercks, J. Jimenez-Barbero and P. H. Seeberger, *J Am Chem Soc*, 2018, **140**, 5421-5426.
14. J. E. Gestwicki, C. W. Cairo, L. E. Strong, K. A. Oetjen and L. L. Kiessling, *J Am Chem Soc*, 2002, **124**, 14922-14933.
15. M. L. Talaga, N. Fan, A. L. Fueri, R. K. Brown, Y. M. Chabre, P. Bandyopadhyay, R. Roy and T. K. Dam, *Biochemistry*, 2014, **53**, 4445-4454.
16. A. Bernardi, J. Jimenez-Barbero, A. Casnati, C. De Castro, T. Darbre, F. Fieschi, J. Finne, H. Funken, K. E. Jaeger, M. Lahmann, T. K. Lindhorst, M. Marradi, P. Messner, A. Molinaro, P. V. Murphy, C. Nativi, S. Oscarson, S. Penades, F. Peri, R. J. Pieters, O. Renaudet, J. L. Reymond, B. Richichi, J. Rojo, F. Sansone, C. Schaffer, W. B. Turnbull, T. Velasco-Torrijos, S. Vidal, S. Vincent, T. Wennekes, H. Zuilhof and A. Imberty, *Chem Soc Rev*, 2013, **42**, 4709-4727.
17. A. Restuccia, M. M. Fettis and G. A. Hudalla, *J Mater Chem B*, 2016, **4**, 1569-1585.
18. M. L. Huang and K. Godula, *Glycobiology*, 2016, **26**, 797-803.
19. C. W. Cairo, J. E. Gestwicki, M. Kanai and L. L. Kiessling, *J Am Chem Soc*, 2002, **124**, 1615-1619.
20. L. L. Kiessling and J. C. Grim, *Chem Soc Rev*, 2013, **42**, 4476-4491.
21. V. Ladmiral, G. Mantovani, G. J. Clarkson, S. Cauet, J. L. Irwin and D. M. Haddleton, *J Am Chem Soc*, 2006, **128**, 4823-4830.
22. T. Ooya, M. Eguchi and N. Yui, *J Am Chem Soc*, 2003, **125**, 13016-13017.
23. B. D. Polizzotti, R. Maheshwari, J. Vinkenborg and K. L. Kiick, *Macromolecules*, 2007, **40**, 7103-7110.
24. C. Xiao, C. Zhao, P. He, Z. Tang, X. Chen and X. Jing, *Macromol Rapid Commun*, 2010, **31**, 991-997.
25. E. Zacco, J. Hutter, J. L. Heier, J. Mortier, P. H. Seeberger, B. Lepenies and B. Koksch, *ACS Chem Biol*, 2015, **10**, 2065-2072.

26. Q. Xiao, S. Zhang, Z. Wang, S. E. Sherman, R. O. Moussodia, M. Peterca, A. Muncan, D. R. Williams, D. A. Hammer, S. Vertesy, S. Andre, H. J. Gabius, M. L. Klein and V. Percec, *Proc Natl Acad Sci U S A*, 2016, **113**, 1162-1167.
27. S. Zhang, Q. Xiao, S. E. Sherman, A. Muncan, A. D. Ramos Vicente, Z. Wang, D. A. Hammer, D. Williams, Y. Chen, D. J. Pochan, S. Vertesy, S. Andre, M. L. Klein, H. J. Gabius and V. Percec, *J Am Chem Soc*, 2015, **137**, 13334-13344.
28. O. S. Caliskan, M. Sardan Ekiz, A. B. Tekinay and M. O. Guler, *Bioconjug Chem*, 2017, **28**, 740-750.
29. G. Gunay, M. Sardan Ekiz, X. Ferhati, B. Richichi, C. Nativi, A. B. Tekinay and M. O. Guler, *ACS Appl Mater Interfaces*, 2017, **9**, 16035-16042.
30. S. S. Lee, T. Fyrner, F. Chen, Z. Alvarez, E. Sleep, D. S. Chun, J. A. Weiner, R. W. Cook, R. D. Freshman, M. S. Schallmo, K. M. Katchko, A. D. Schneider, J. T. Smith, C. Yun, G. Singh, S. Z. Hashmi, M. T. McClendon, Z. Yu, S. R. Stock, W. K. Hsu, E. L. Hsu and S. I. Stupp, *Nat Nanotechnol*, 2017, **12**, 821-829.
31. J. Liu, Z. Sun, Y. Yuan, X. Tian, X. Liu, G. Duan, Y. Yang, L. Yuan, H. C. Lin and X. Li, *ACS Appl Mater Interfaces*, 2016, **8**, 6917-6924.
32. S. Ustun Yaylaci, M. Sardan Ekiz, E. Arslan, N. Can, E. Kilic, H. Ozkan, I. Orujalipoor, S. Ide, A. B. Tekinay and M. O. Guler, *Biomacromolecules*, 2016, **17**, 679-689.
33. Y. Ruff, E. Buhler, S. J. Candau, E. Kesselman, Y. Talmon and J. M. Lehn, *J Am Chem Soc*, 2010, **132**, 2573-2584.
34. A. Nelson, J. M. Belitsky, S. Vidal, C. S. Joiner, L. G. Baum and J. F. Stoddart, *J Am Chem Soc*, 2004, **126**, 11914-11922.
35. D. W. Lee, T. Kim, I. S. Park, Z. Huang and M. Lee, *J Am Chem Soc*, 2012, **134**, 14722-14725.
36. G. Thoma, M. B. Streiff, A. G. Katopodis, R. O. Duthaler, N. H. Voelcker, C. Ehrhardt and C. Masson, *Chemistry*, 2005, **12**, 99-117.
37. V. Percec, P. Leowanawat, H. J. Sun, O. Kulikov, C. D. Nusbaum, T. M. Tran, A. Bertin, D. A. Wilson, M. Peterca, S. Zhang, N. P. Kamat, K. Vargo, D. Moock, E. D. Johnston, D. A. Hammer, D. J. Pochan, Y. Chen, Y. M. Chabre, T. C. Shiao, M. Bergeron-Brlek, S. Andre, R. Roy, H. J. Gabius and P. A. Heiney, *J Am Chem Soc*, 2013, **135**, 9055-9077.
38. A. Restuccia, Y. F. Tian, J. H. Collier and G. A. Hudalla, *Cell Mol Bioeng*, 2015, **8**, 471-487.
39. J. P. Jung, J. Z. Gasiorowski and J. H. Collier, *Biopolymers*, 2010, **94**, 49-59.
40. J. P. Jung, A. K. Nagaraj, E. K. Fox, J. S. Rudra, J. M. Devgun and J. H. Collier, *Biomaterials*, 2009, **30**, 2400-2410.
41. R. R. Pompano, J. Chen, E. A. Verbus, H. Han, A. Fridman, T. McNeely, J. H. Collier and A. S. Chong, *Adv Healthc Mater*, 2014, **3**, 1898-1908.
42. W. S. Hlavacek, R. G. Posner and A. S. Perelson, *Biophys J*, 1999, **76**, 3031-3043.
43. C. Portillo-Tellez Mdel, M. Bello, G. Salcedo, G. Gutierrez, V. Gomez-Vidales and E. Garcia-Hernandez, *Biophys J*, 2011, **101**, 1423-1431.
44. C. S. Wright, *J Biol Chem*, 1992, **267**, 14345-14352.
45. O. S. Makin and L. C. Serpell, *FEBS J*, 2005, **272**, 5950-5961.
46. T. K. Dam and C. F. Brewer, *Biochemistry*, 2008, **47**, 8470-8476.
47. T. K. Dam, T. A. Gerken and C. F. Brewer, *Biochemistry*, 2009, **48**, 3822-3827.
48. J. Lazar, H. Park, R. R. Rosencrantz, A. Boker, L. Elling and U. Schnakenberg, *Macromol Rapid Commun*, 2015, **36**, 1472-1478.
49. P. N. Lyer, K. D. Wilkinson and L. J. Goldstein, *Arch Biochem Biophys*, 1976, **177**, 330-333.
50. S. Nakamura-Tsuruta, J. Kominami, M. Kamei, Y. Koyama, T. Suzuki, M. Isemura and J. Hirabayashi, *J Biochem*, 2006, **140**, 285-291.
51. K. Zhu, R. A. Bressan, P. M. Hasegawa and L. L. Murdock, *FEBS Lett*, 1996, **390**, 271-274.
52. T. Hasegawa, S. Kondoh, K. Matsuura and K. Kobayashi, *Macromolecules*, 1999, **32**, 6595-6603.
53. J. Kumar, L. McDowall, G. J. Chen and M. H. Stenzel, *Polym Chem-Uk*, 2011, **2**, 1879-1886.
54. D. Schwefel, C. Maierhofer, J. G. Beck, S. Seeberger, K. Diederichs, H. M. Moller, W. Welte and V. Wittmann, *J Am Chem Soc*, 2010, **132**, 8704-8719.
55. G. M. Consoli, F. Cunsolo, C. Geraci and V. Sgarlata, *Org Lett*, 2004, **6**, 4163-4166.
56. M. Fiore, N. Berthet, A. Marra, E. Gillon, P. Dumy, A. Dondoni, A. Imberty and O. Renaudet, *Org Biomol Chem*, 2013, **11**, 7113-7122.
57. C. Maierhofer, K. Rohmer and V. Wittmann, *Bioorg Med Chem*, 2007, **15**, 7661-7676.
58. G. Bains, R. T. Lee, Y. C. Lee and E. Freire, *Biochemistry*, 1992, **31**, 12624-12628.
59. B. Gastman, K. Wang, J. Han, Z. Y. Zhu, X. Huang, G. Q. Wang, H. Rabinowich and E. Gorelik, *Biochem Biophys Res Commun*, 2004, **316**, 263-271.
60. M. Reynolds, M. Marradi, A. Imberty, S. Penades and S. Perez, *Glycoconj J*, 2013, **30**, 747-757.
61. X. Wang, O. Ramstrom and M. Yan, *Anal Chem*, 2010, **82**, 9082-9089.
62. J. Z. Gasiorowski and J. H. Collier, *Biomacromolecules*, 2011, **12**, 3549-3558.
63. G. A. Hudalla, T. Sun, J. Z. Gasiorowski, H. Han, Y. F. Tian, A. S. Chong and J. H. Collier, *Nat Mater*, 2014, **13**, 829-836.
64. M. M. Fettis, Y. H. Wei, A. Restuccia, J. J. Kurian, S. M. Wallet and G. A. Hudalla, *J Mater Chem B*, 2016, **4**, 3054-3064.

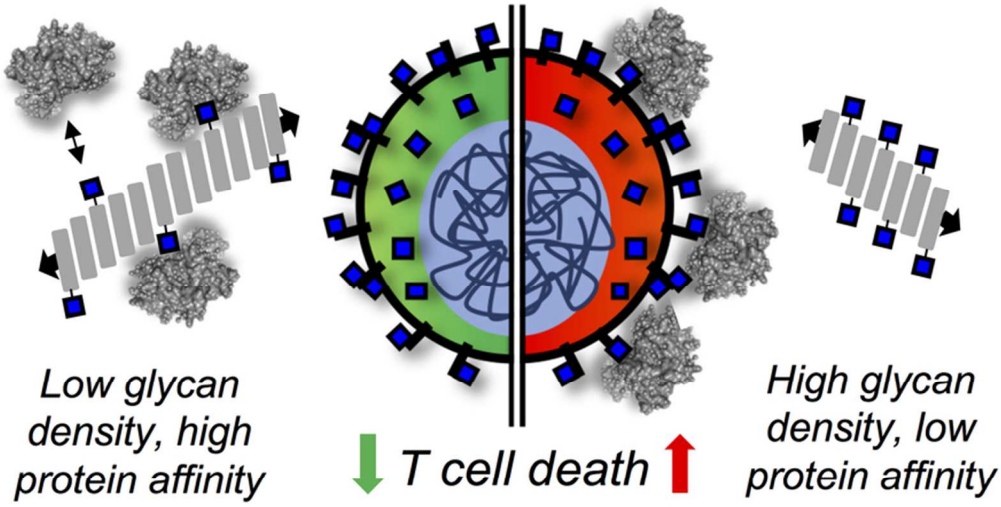

Efficacy of glycosylated β-sheet peptide nanofibers to inhibit carbohydrate-binding proteins can be increased by tuning carbohydrate density to maximize protein binding affinity.

73x63mm (300 x 300 DPI)